Supporting Information

Comparative Evaluation of the Power-to-Methanol Process Configurations and Assessment of Process Flexibility

Siphesihle Mbatha[a,c,*], Xiaoti Cui[e], Payam G. Panah[e], Sébastien Thomas[b], Ksenia Parkhomenko[b], Anne-Cécile Roger[b], Benoit Louis[b], Ray Everson[c], Paulo Debiagi[f], Nicholas Musyoka[f], Henrietta Langmi[d]

[a] *HySA Infrastructure Centre of Competence, Centre for Nanostructures and Advanced Materials (CeNAM), Chemicals Cluster, Council for Scientific and Industrial Research (CSIR), Pretoria 0001, South Africa*

[b] *Institute of Chemistry and Processes for Energy, Environment and Health (ICPEES), UMR 7515 CNRS-University of Strasbourg, 25 rue Becquerel, Strasbourg 67087 Cedex 02, France*

[c] *Centre of Excellence in Carbon Based Fuels, School of Chemical and Minerals Engineering, Faculty of Engineering, North-West University, Private Bag X6001, Potchefstroom, 2531, South Africa*

[d] *Department of Chemistry, University of Pretoria, Private Bag X20, Hatfield, 0028, South Africa*

[e] *Department of Energy, Aalborg University, Pontoppidanstr. 111, 9220 Aalborg, Denmark*

[f] *Nottingham Ningbo China Beacons of Excellence Research and Innovation Institute, University of Nottingham Ningbo China, Ningbo 315100, PR China*

*Correspondence Emails: siphe.mbatha94@gmail.com

ABSTRACT

This paper compares different power-to-methanol process configurations encompassing electrolyser, adiabatic reactor (s) and methanol purification configurations. Twelve different power-to-methanol configurations based on direct CO_2 hydrogenation with H_2 derived from H_2O-electrolysis were modelled, compared, and analysed. High temperature solid oxide electrolyser is used for hydrogen production. Fixed bed reactor is used for methanol synthesis. The aim of the paper is to give detailed comparison of the process layouts under similar conditions and select the best performing process configuration considering the overall methanol production, CO_2 conversion, flexibility, and energy efficiency. ASPEN PLUS® V11 is used for flowsheet modelling and the system architectures considered are the open loop systems where methanol is produced at 100 kton/annum and sold to commercial wholesale market as the final purified commodity. Further optimization requirements are established as targets for future work. Three options of power-to-methanol configuration with methanol synthesis from CO_2 hydrogenation are proposed and further evaluated considering process flexibility. From the evaluation, the series-series based configuration with three adiabatic reactors in series performed better in most parameters including the flexible load dependent energy efficiency.

Keywords: Power-to-Methanol System Configurations, Process Design, Process Integration, Solid Oxide Electrolyser.

Section A1: Thermodynamic model selection

In this work, RKSMHV2 is selected as the thermodynamic model. It is an Aspen built-in physical property model that is suitable to describe the mixture properties of non-polar and polar compounds, in combination with light gases. It is flexible and predictive, which do not require any binary interaction parameters obtained from experiment. In general, this model extends the RKS (Redlich-Kwong-Soave) equation of state by incorporating the Lyngby modified UNIFAC model to calculate the excess Gibbs free energy for the liquid phase using MHV2 (second order modified Huron-Vidal) mixing rules. The MHV2 mixing rules predict the binary interactions at any pressure. Using the Lyngby modified UNIFAC model, the Redlich-Kwong-Soave MHV2 model is predictive for any interaction that can be predicted by Lyngby modified UNIFAC at low pressure. RKSMHV2 property method can be used up to high temperatures and pressures (e.g. 150 bar). All the binary interaction parameter values needed for this model were provided by Aspen Plus™ library.

This model was used by Van-Dal and Bouallou[8] to design their methanol process. In addition, another previous similar contribution by Luyben[9] used the "RK-Aspen" model, which is also a flexible and predictive thermodynamic model being similar to RKSMHV2. Recently this model has been used to model both steam and co-electrolysis process for methanation studies by Patcharavorachot et al.[6] using SOEC operating at atmospheric pressure conditions. From their validation results they deduced that " The prediction results from the SOEC model fit well with the experimental data. Considering R-squared, the predictive R^2 of H_2 and CO are in the range of 0.981–0.992 and 0.997–0.998, respectively. R^2 values of the SOEC model are close to 1 which indicates that the predicted results from the SOEC model are reliable and acceptable." The components in the SOEC technology are hydrogen, water/steam, CO_2, CO and oxygen. Water/steam is a polar compound which is capable of bonding (associating) with hydrogen and the water/steam will be mixed with hydrogen at the SOE outlet. The gas solubilities are significantly better predicted by RKSMHV2. Notably, RKSMHV2 predicts the gas solubility into methanol with less error. For more details on gas solubility predictions, at various pressure, the reader is referred to the supplementary work of Chiou et al.[7]. The reader an also see the wide pressure predictive capability of the model. It is also noted by Chiou et al.[7] that both

RKSMHV2 predict the gas solubility into water with great deviation. However, the solubility of CO_2 and H_2 into water is much less than those into methanol. Hence, these deviations are treated as non-consequential to process simulation as also deduced by Chiou et al.[7].

Section A2: Reaction kinetic validation for methanol synthesis

In this study, the reaction kinetic model by Van den Bussche and Froment[1] was selected to calculate the reaction rates in the methanol reactors under the investigated conditions with the following equations (shown in Table S1) for reaction (2) and reaction (3) considered in this study.

Table S1. Reaction kinetics.

Reaction kinetics	No.	Ref.
$r_{MeOH} = k_d \frac{P_{CO2}P_{H2} - K_1^{-1}P_{H2O}P_{MeOH}/P_{H2}^2}{(1 + k_cP_{H2O}/P_{H2} + k_aP_{H2}^{0.5} + k_bP_{H2O})^3}$	(1)	[1]
$r_{RWGS} = k_e \frac{P_{CO2} - K_2P_{H2O}P_{CO}/P_{H2}}{1 + k_cP_{H2O}/P_{H2} + k_aP_{H2}^{0.5} + k_bP_{H2O}}$	(2)	
$K_1 = 10^{-10.592 + \frac{3066}{T}} \approx \exp(-24.389 + \frac{7059.726}{T})$	(3)	[2]
$K_2 = 10^{2.029 + \frac{-2073}{T}} \approx \exp(-4.672 + \frac{4773.26}{T})$	(4)	

where the kinetic factors k_d and k_e, and the adsorption constants k_a, k_b and k_c were calculated with parameters shown in Table S2.

Table S2. Parameters for the kinetic equations.

$k = A \cdot e^{B/RT}$	A	B
k_a [bar$^{-0.5}$]	0.499	17197
k_b [bar^{-1}]	6.62×10^{-11}	124119
k_c [—]	3453.38	-
k_d [mole/(kg·s·bar^2]	1.07	36696
k_e [mole/(kg·s·bar]	1.22×10^{10}	−94765

The parameter values above were adjusted for the input values in Aspen PLUS due to the unit difference and the adjusted values are shown in Table S3. The units of bar, kmol and kmol/(kg_{cat}·s) were used for the pressure, mole flow and reaction rate, respectively. Parameter settings with different units may also be used in Aspen plus e.g. Pascal was used for pressure in the literature.[3]

Table S3. The input values in Aspen plus for the kinetic equations.

$k_i = k \cdot exp(-E/RT)$	k	E
k_d	0.00107, kmol/(kg_{cat}·s·bar^2)	−36696, kJ/kmol

k_e	1.22×10^7, kmol/(kg_{cat}·s·bar)	94765, kJ/kmol

$lnK_i = A_i+B_i/T$	A_i	B_i
$ln(1/K_1)$	24.389	−7059.726
lnK_2	−4.762	4773.16
lnK_a	−0.695149	2068.44
lnK_b	-23.438	14928.92
lnK_c	8.14711	-

The methanol reactor model developed by using Aspen Plus was validated by comparing with the simulation results in Van den Bussche and Froment[1]. Good agreement was shown in Fig. S1. The operating conditions for the simulation of the methanol reactor were also given in Van den Bussche and Froment[1].

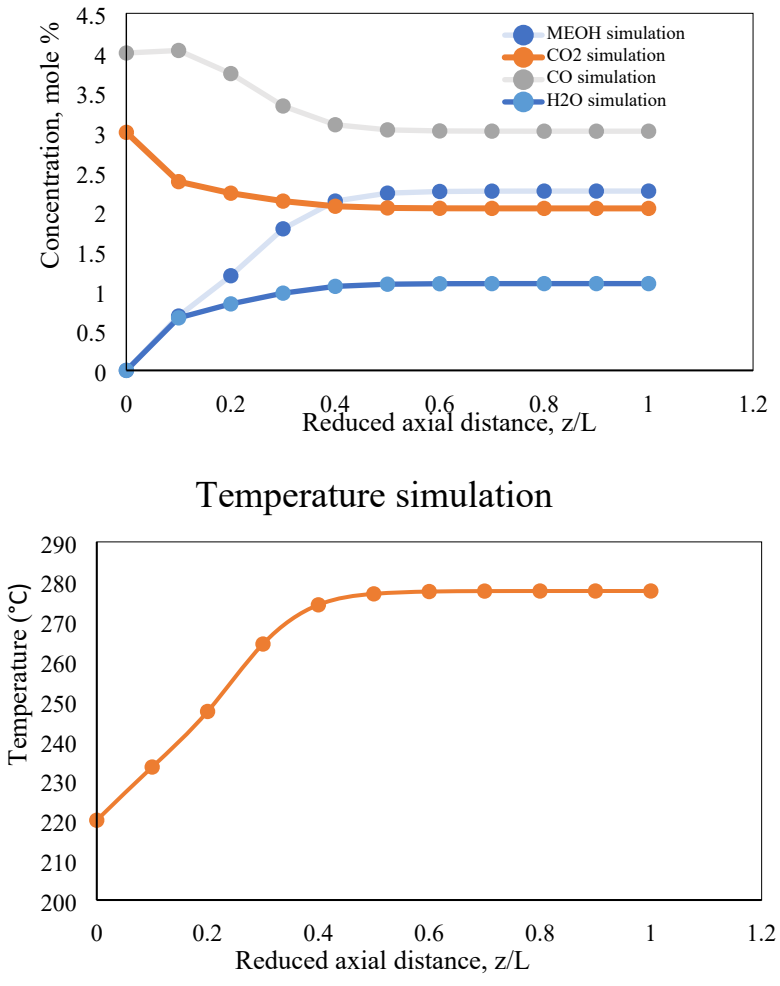

Figure S2. (a) Gas composition and (b) temperature profiles along the methanol reactor under the operation conditions in Van den Bussche and Froment[1].

Ergun equation

The pressure drop over the catalyst bed was evaluated by the following Ergun equation[4]:

$$\frac{dP}{dz} = -\left(1.75 + 150\frac{1-\varepsilon}{Re_p^s}\right)\frac{1-\varepsilon}{\varepsilon^3}\frac{\rho_f u^2}{d_p^s} \quad (5)$$

Section A3: Other Considered flowsheets

It is important to highlight all flowsheet comprises a recycle loop, and the SOEC flowsheet was fixed for better comparison. Figure S3 illustrates flowsheet 1in which a single adiabatic reactor is used, and this is taken as the base flowsheet as it is typically the most investigated scheme in literature.[7] Flowsheet 2, illustrated in Figure S4, is modified from the work of Kiss et al. and comprises the stripper unit mounted before the reactor to remove water from wet hydrogen for the purpose of preventing catalyst deactivation.[11] Flowsheet 3, illustrated in Figure S5, comprises two adiabatic reactors in series and with intermediate cooling and separation of methanol and water at 45 bar and 35°C. The other feature of flowsheet S3 is the addition of compressor to the feed of the second reactor to raise the operating pressure of the second reactor to the same pressure as the first reactor in the scheme.

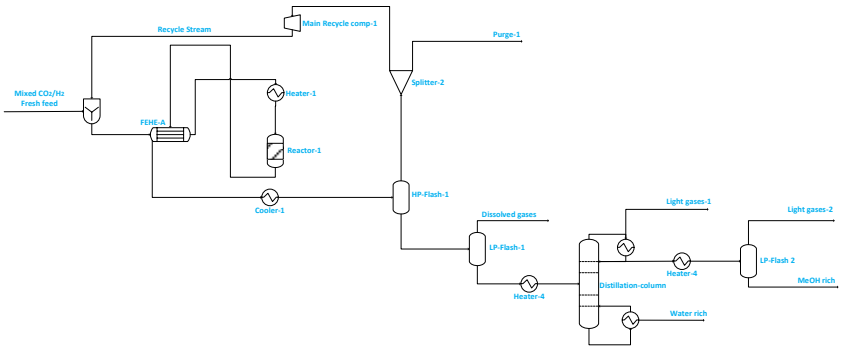

Figure S3: Illustrates Flowsheet 1 in which a single reactor is used, and this is taken as the base flowsheet.

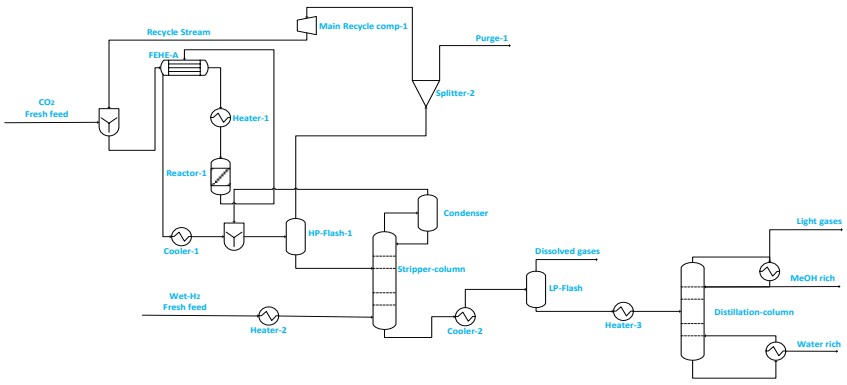

Figure S4: Illustration of Flowsheet 2. This flowsheet features a stripper column and wet hydrogen.

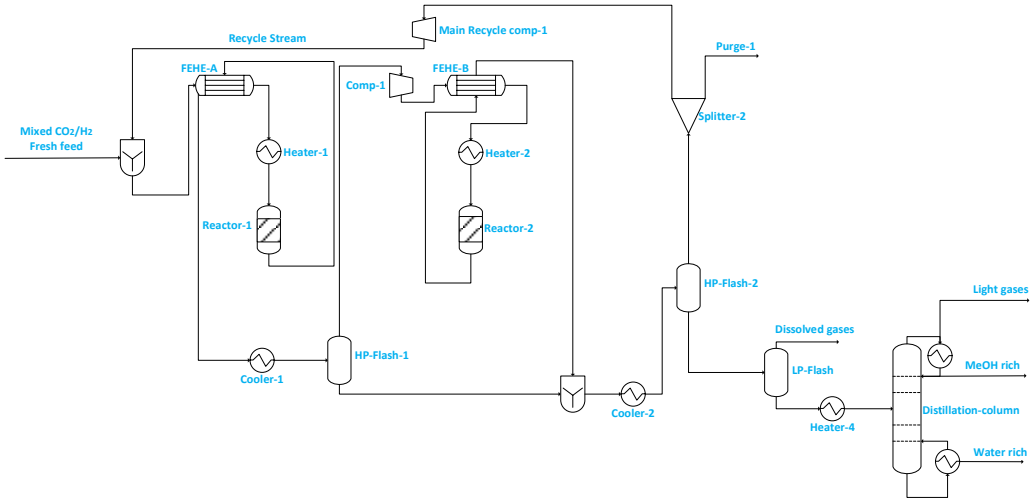

Figure S5: Illustration of Flowsheet 3. This flowsheet comprises two reactors in series and with intermediate cooling and separation of methanol and water at 45 bar and 35°C. The other feature of flowsheet 3 is the addition of compressor on the feed to the second reactor.

Flowsheet 4 illustrated in Figure S6 includes two reactors in series but with a wash column which uses $C_3H_8O_3$ as a solvent mounted in the position after the first reactor followed by separation and two distillation columns in which the first is used for solvent recovery while the second distillation column is used for methanol purification. The design of the separation in flowsheet 4 attempts to reduce as much as possible vented residual gases and to push the driving force reaction to methanol by elm iminating as much as possible the water and methanol from the unconverted gases coming up from the first reactor.

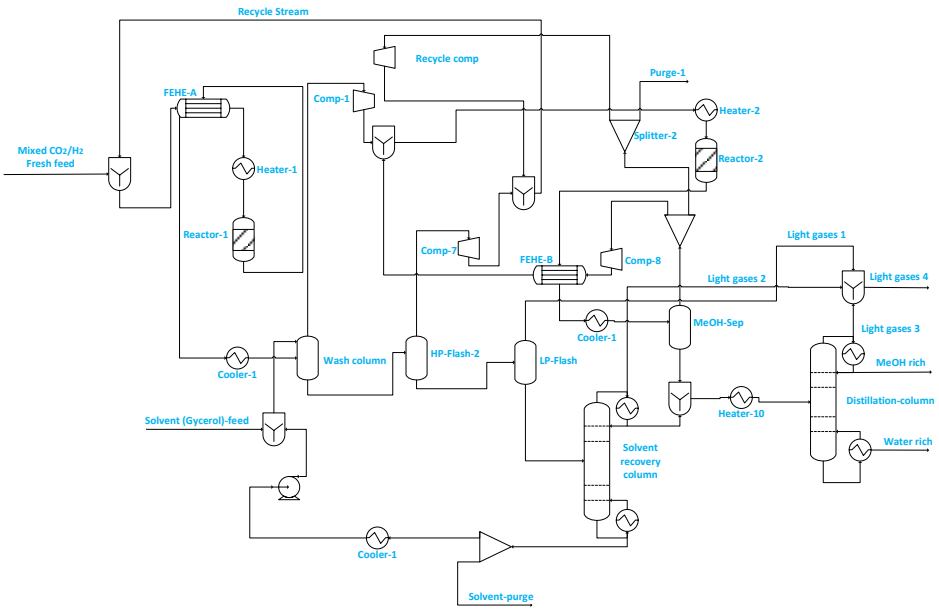

Figure S6: Illustration of Flowsheet 4. This flowsheet features a wash column and two distillation units.

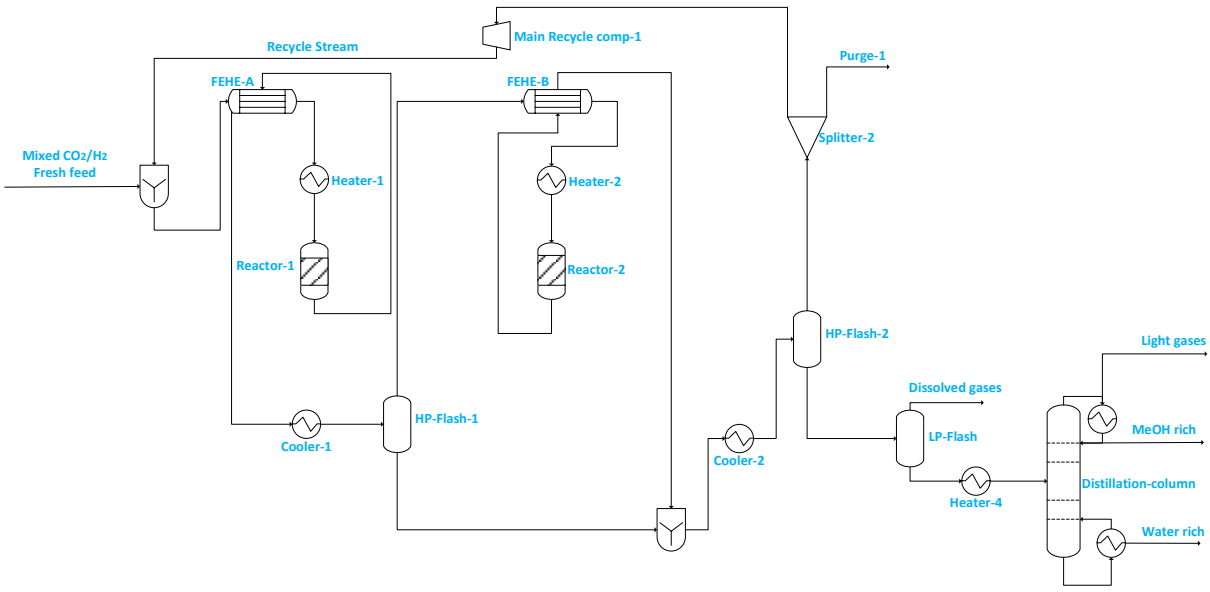

Figure S7: Illustration of Flowsheet 5. This flowsheet assumes limited system pressure drop in the methanol section.

Flowsheet 5 illustrated in Figure S7 closely resembles flowsheet 3 with two reactors in series but with a change in operation of the intermediate separator which is operated at pressure equal to the reactor pressure to avoid the compression of the feed to the second reactor which comprises unconverted gases and some fraction of methanol. Furthermore, the separator placed after the second reactor which removes the unconverted gases from the stream sent to distillation is operated at higher pressure and thus reduces the compression work.

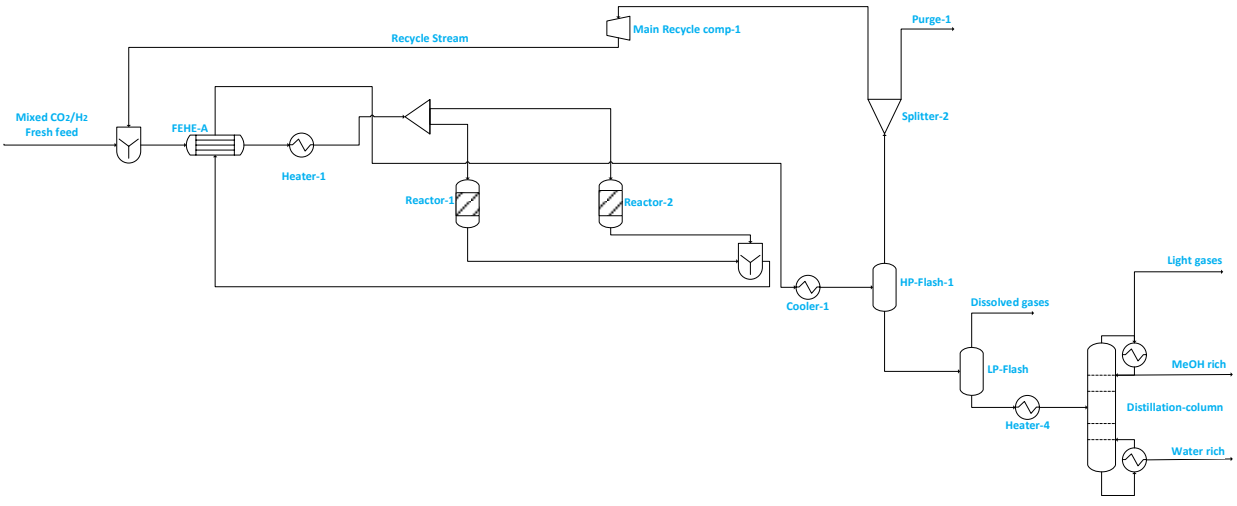

Figure S8: Illustration of Flowsheet 6A. This features two reactors in parallel with long recycle reactor allowing the first reactor to get the mix of recycle and fresh feed.

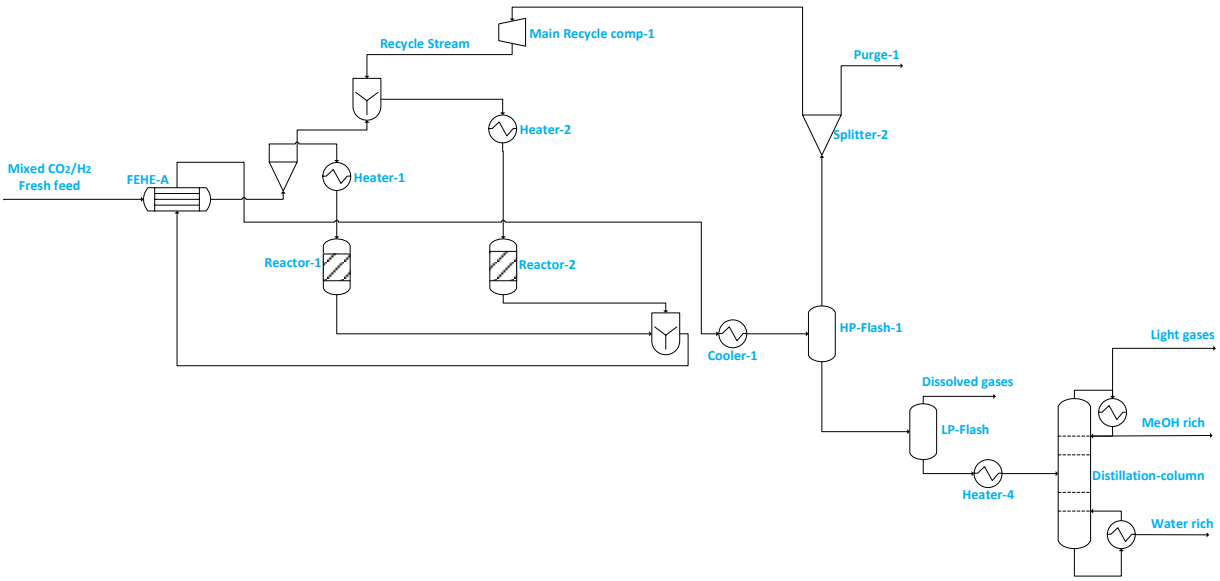

Figure S9: Illustration of Flowsheet 6B. This features two reactors in parallel with short recycle to second reactor allowing the first reactor to get only the fresh feed.

Flowsheet 6A and 6B illustrated in Figure S8 and S9, respectively, has two reactors connected in parallel. Flowsheet 6A has a long recycle to both reactors and therefore a feed (comprising fresh feed and recycle) split at 50% to both reactors, while for flowsheet 6B the fresh feed flow is split to 50% and the portion of the fresh feed to the second reactor in flowsheet 6B is mixed with all the recycle of unconverted gases whereas the portion to the first reactor is kept as fresh feed.

Section A4: Flowsheets controls, design sensitivity and heat integration

A4.1 Flowsheets with control loops used in dynamic modelling

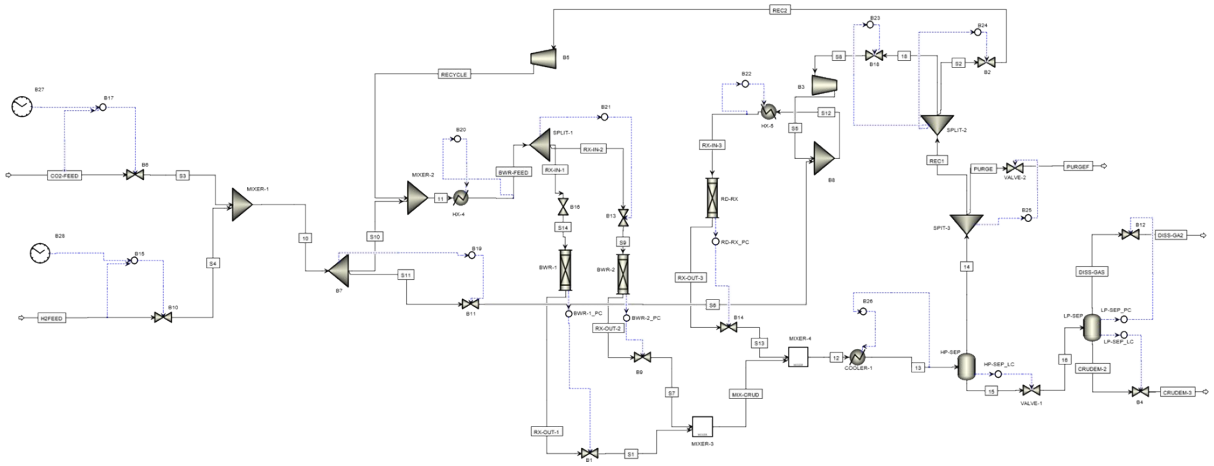

Figure S10: Flowsheet 7

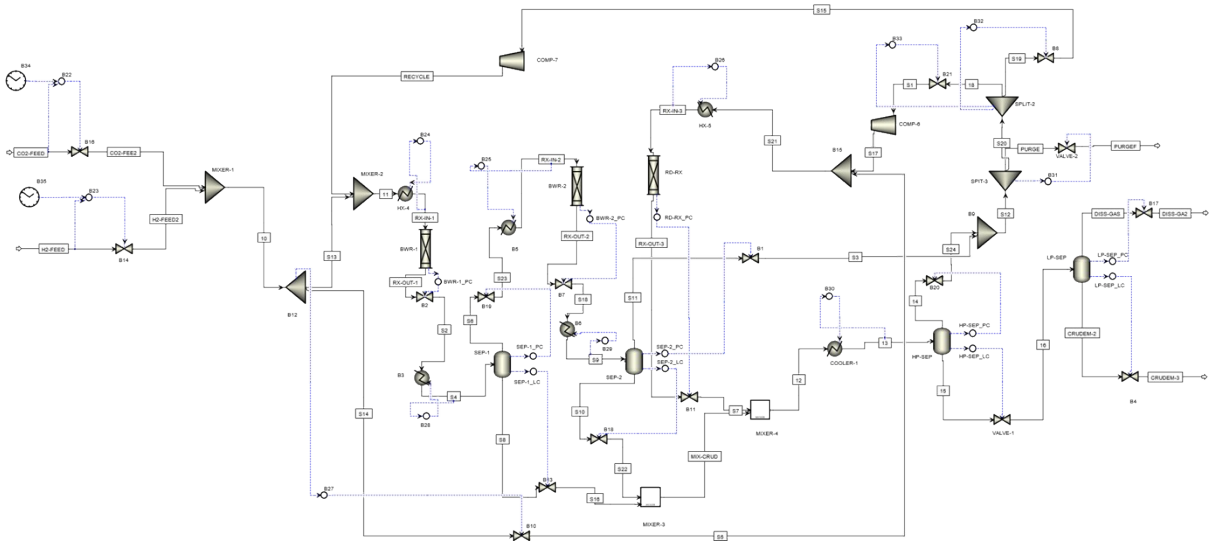

Figure S11: Flowsheet 7B

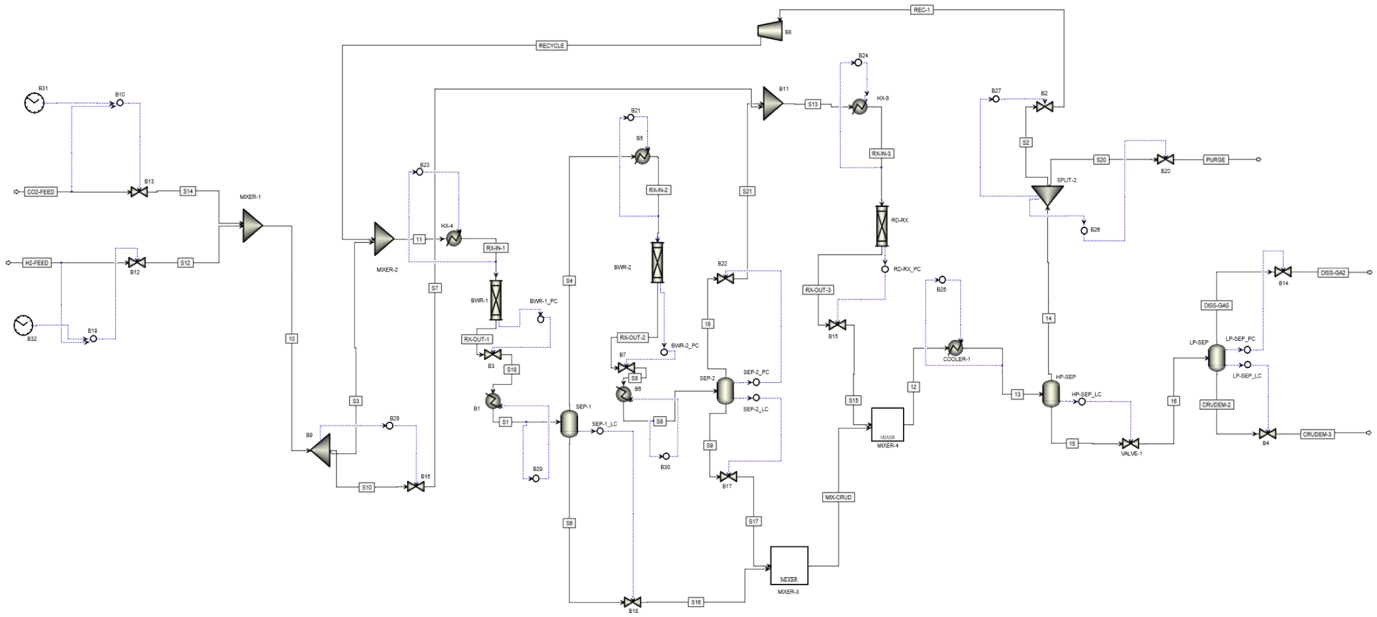

Figure S12: Flowsheet 8

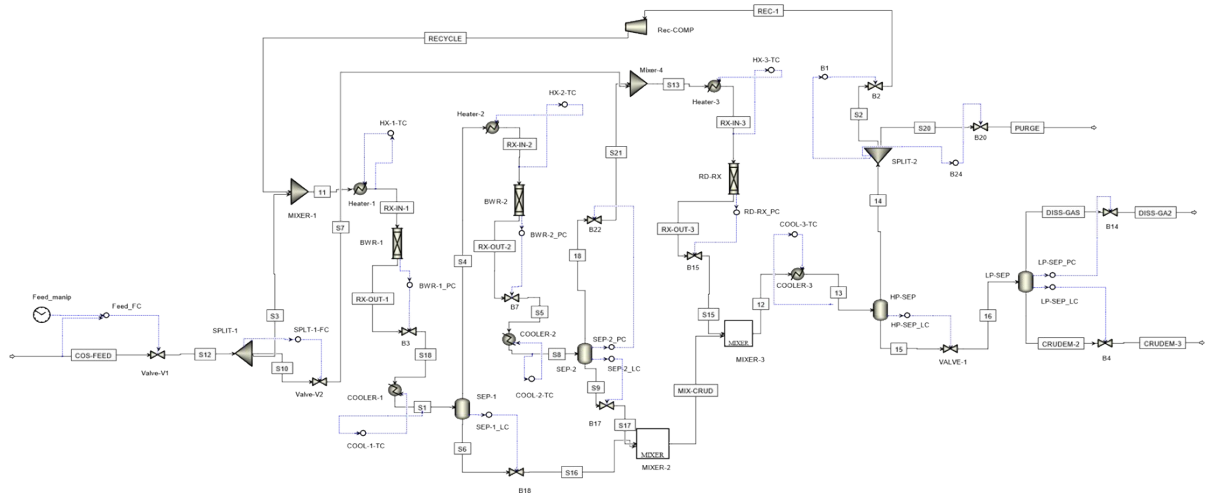

Figure S13: Co-electrolysis flowsheet

All controllers in the model are proportional – integral (PI) type and were tuned based on the rule of Zigler-Nichols by automatic relay feedback test in Aspen plus dynamics. There are two types of control action i.e., direct, and reverse control. Direct action ensures that when the value of the measured variable increases, the value of the manipulated variables also increases. The reverse action mode ensures that the value of measured variables decreases resulting in the increase of manipulated value.[5] Auto-mode controllers are straightforward, which means that when there is a difference between manipulated variable and set point, actuator would act to compensate the difference corresponding to the specified control action.[5] Auto-controllers are used in level control of the flash drums.

Table S5: The description of the controllers in dynamic modelling for the parallel-series flowsheet 7 system

Controller	Controller Objectives	Actuator	Range of change	P	I	Control Action
B15	H_2-Feed flowrate	Valve B10	0-100 %	1.4	2	Reverse
B17	CO_2-feed flowrate	Valve B6	0-100 %	2	2	Reverse
B19	Fresh feed split ratio to reactors	Valve B11	0-100 %	1	4	Direct
B20	Reactor BWR-1 inlet temperature	HX-4	0-440 °C	1	4	Reverse
B21	Total feed split ratio to reactors BWR-1 & 2	Valve B13	0-100 %	4.4	2	Direct
B22	Reactor BWR-2 inlet temperature	HX-5	0-440 °C	1	2	Reverse
B23	Ratio of the recycle flow for the recycle stream S18 to reactor RD-RX	Valve B18	0-100 %	1	2	Reverse
B24	Ratio of purging flow for total recycle stream S2	Valve B2	0-100 %	1.2	2	Direct
B25	Ratio of purging flow for PURGE stream	Valve-2	0-100 %	1	2	Reverse
B26	HP-SEP feed cooler temperature	Cooler-1	0-76 °C	1	2	Reverse
BWR-1_PC	Reactor BWR-1 pressure	Valve B1	0-100%	20	4	Direct
BWR-2_PC	Reactor BWR-2 pressure	Valve B9	0-100%	19	4	Direct
RD-RX_PC	Reactor RD-RX pressure	Valve B14	0-100%	46	4	Direct

Table S6. The description of the controllers in dynamic modelling for the series-series flowsheet 7B system

Controller	Controller objectives	Actuator	Range of change	P	I	Control Action
B22	H2-feed flowrate	Valve B16	0-100 %	8	5	Reverse
B23	CO2-feed flowrate	Valve B14	0-100 %	8	20	Reverse
B24	Reactor BWR-1 inlet temperature	HX-4	0-440 °C	1	2	Reverse
B25	Reactor BWR-2 inlet temperature	HX B5	0-440 °C	1	2	Reverse
B26	Reactor RD-RX inlet temperature	HX-5	0-440 °C	3	1	Reverse
B27	Fresh feed split ratio to reactors	Valve B10	0-100%	1	1	Reverse
B28	SEP-1 feed cooler	Cooler B3	0-60 °C	1	1	Reverse

Controller	Controller objectives	Actuator	Range of change	P	I	Control Action
	temperature					
B29	SEP-2 feed cooler temperature	Cooler B6	0-60 °C	1	1	Reverse
B30	HP-SEP feed cooler temperature	Cooler-1	0-78 °C	1	1	Reverse
B31	Ratio of purging flow for PURGE stream	Valve-2	0-100 %	1	2	Reverse
B32	Ratio of the recycle flow for the total recycle stream S19	Valve B8	0-100 %	60	5	Direct
B33	Ratio of the recycle flow for the recycle stream S18 to reactor RD-RX	Valve B21	0-100 %	60	5	Reverse
BWR-1_PC	Reactor BWR-1 pressure	Valve B2	0-100 %	200	60	Direct
BWR-2_PC	Reactor BWR-2 pressure	Valve B7	0-100 %	200	60	Direct
RD-RX_PC	Reactor RD-RX pressure	Valve B11	0-100%	200	60	direct

Table S7. The description of the controllers in dynamic modelling for series-series flowsheet 8 system

Controller	Controller objectives	Actuator	Range of change	P (%/%)	I(min)	Control Action
B19	CO_2 flowrate	Valve B12	0-100%	1	2	Reverse
B10	H_2 flowrate	Valve B13	0-100%	1	2	Reverse
B21	Reactor BWR-2 inlet temperature	HX B5	0-440 °C	1	2	Reverse
B23	Reactor BWR-1 inlet temperature	HX-4	0-440 °C	1	2	Reverse
B24	Reactor RD-RX inlet temperature	HX-5	0-440 °C	1	20	Reverse
B25	HP-separator feed cooler-1 temperature	Cooler-1	0-116 °C	1	2	Reverse
B26	Ratio of purging flow for PURGE stream	Valve B20	0-100%	1	2	Reverse
B27	Ratio of the recycle flow for the recycle stream REC-1	Valve B2	0-100%	1	2	Direct
B28	Fresh feed split ratio to reactors	Valve B16	0-100%	1	2	Direct
B29	SEP-1 feed cooler-1 temperature	Cooler B1	0-60 °C	1	2	Reverse
B30	SEP-2 feed cooler-1 temperature	Cooler B6	0-60 °C	1	2	Reverse
BWR-1_PC	Reactor BWR-1 pressure	Valve B3	0-100%	10	12	Direct
BWR-2_PC	Reactor BWR-1 pressure	Valve B7	0-100%	10	12	Direct
RD-RX_PC	Reactor RD-RX pressure	HX-5	0-100%	10	12	Direct

Table S8. The description of the controllers in dynamic modelling for the co-electrolysis system

Controller	Controller objective	Actuator	Range of change	P (%/%)	I(min)	Control Action
Feed_FC	Syngas feed flowrate	Valve -V1	0-100 %	150	0.5	Reverse
SPLT-1-FC	Fresh feed split ratio to reactors	Valve -V2	0-100 %	1	2	Reverse
HX-1-TC	Reactor BWR-1 inlet temperature	Heater-1	0-362 °C	2	2	Reverse
HX-2-TC	Reactor BWR-2 inlet temperature	Heater-2	0-362 °C	2	2	Reverse
HX-3-TC	Reactor RD-RX inlet temperature	Heater-3	0-385 °C	2	2	Reverse
B1	Ratio of the recycle flow for the recycle stream REC-1	Valve B2	0-100 %	1	15	Direct
B24	Ratio of the recycle flow for the recycle stream REC-1	Valve B20	0-100 %	2	0.5	Reverse
COOL-1-TC	SEP-1 feed cooler-1 temperature	COOLER-1	0-60 °C	2	2	Reverse
COOL-2-TC	SEP-2 feed cooler-2 temperature	COOLER-2	0-60 °C	2	2	Reverse
COOL-3-TC	HP-SEP feed cooler-3 temperature	COOLER-3	0-60 °C	1	2	Reverse
BWR-1_PC	Reactor BWR-1 pressure	Valve B3	0-100 %	2	2	Direct
BWR-2_PC	Reactor BWR-2 pressure	Valve B7	0-100 %	2	2	Direct
RD-RX_PC	Reactor RD-RX pressure	Valve B15	0-100 %	2	2	Direct

A4.2: Design-based sensitivity analysis

A4.2.1 Effect of recycle, reactor temperature and length, separator pressure and temperature on the overall methanol production.

Recycle ratio is an effective control parameter of the process (particularly the reactor) productivity and temperature. For the parallel configuration, Figure 14(a) shows that the feed to reactor 3 (its fraction equal to 1-recycle) which is in series with the two parallel reactors must be reduced. This means that the recycle to the parallel reactors must be increased to enhance the production of methanol. In other words, recycling 90% of the unconverted gases, in the absence of inert, to the parallel configuration increases the methanol production rate. This effect is prevalent in all flow configuration, including the case of series reactors with recycle which tends to favour the choice of long recycle. The effect of separator pressure on methanol production shows a decrease in methanol production as the pressure of the separator is increased at constant temperature. This is one of the key parameters in the design and optimization of the PtMeOH process as the combination of separation pressure and methanol production rate affects the profit of the process, predominantly in the case where the recirculation stream of unconverted gases is included. Following the effect of pressure on overall methanol production, as observed in Figure 14(b) above, the temptation would be to operate the separator at low pressure as possible. However, this increases the recycle gas compression and renders the process less energy efficient and costly.

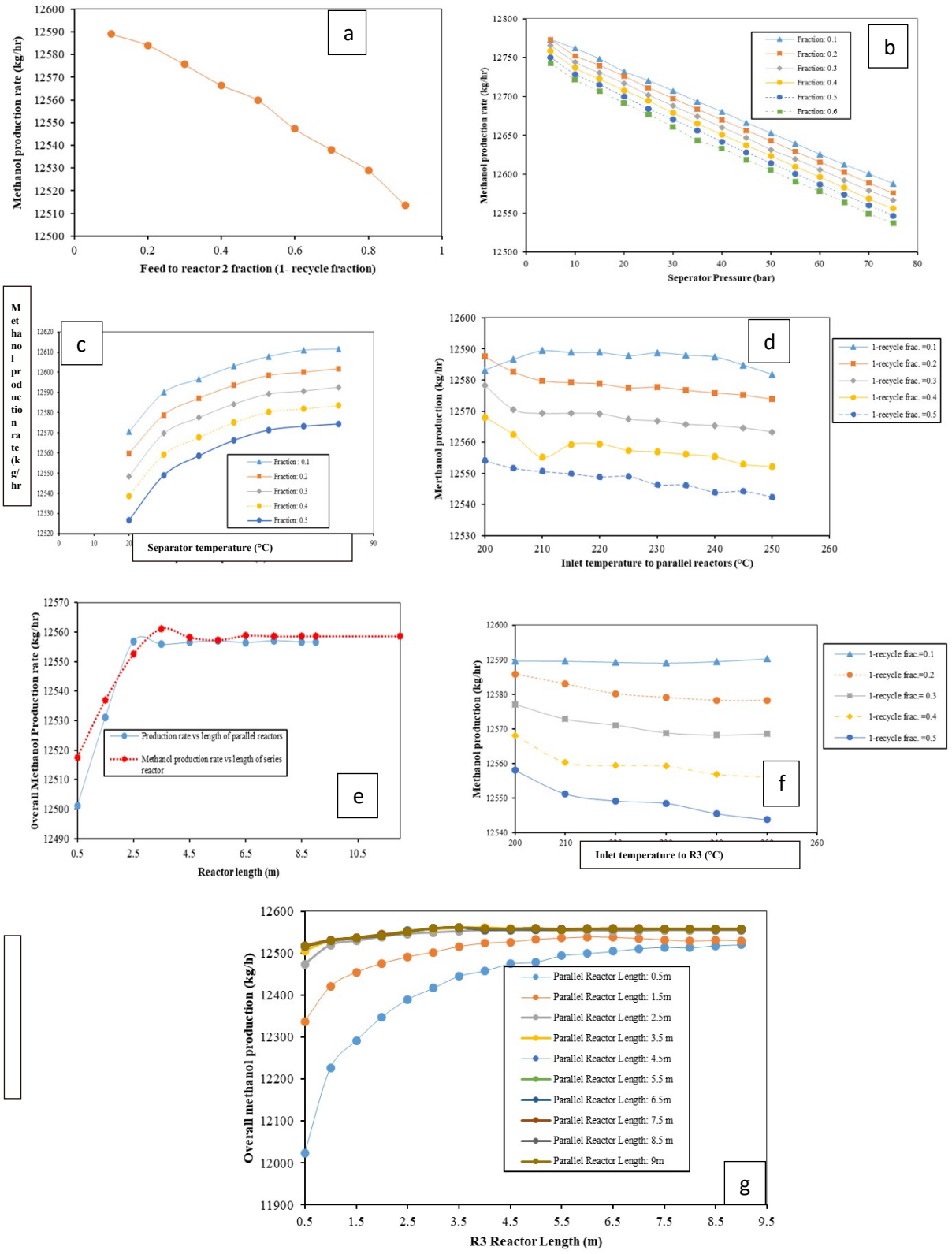

Figure S14: (a) Illustration of effect of recycle (flowsheet 7), (b) Effect of separator pressure on the overall methanol production rate (flowsheet 7) at variable feed to reactor 3 fractions (denoted as 1-Recycle). The temperature of the separator in this sensitivity analysis was kept at T=38 °C. (c) Effect of separator temperature on the methanol production rate at variable feed to reactor 3 fractions (denoted as 1-Recycle). The pressure of the separator for this analysis was kept at P=73.4 bar. (d) Effect of varying

the inlet temperature to parallel reactors. (e) Effect of varying the length of the reactor on the methanol production rate. (f) Effect of varying the inlet temperature to reactor 3. For this sensitivity the fraction =1-recycle was kept at fraction =0.5. (g) Effect of varying length of the reactor on the methanol production rate. Here the series reactor and parallel reactor length are varied. Since the split ratio between the parallel reactors is 50%, the parallel reactors are taken to have equal length. In addition, for this sensitivity, the fraction =1-recycle was kept at fraction = 0.5.

Should catalysts be improved to achieve very high conversion or operate at significantly lower pressure, separator pressure can be subsequently reduced, and this will improve the separation cost/ efficiency. Lowering the pressure of the separator increases the overall methanol production rate. While increasing the separator temperature only yields marginal increase in the overall methanol production rate, as shown in Figure 14 (c). This is an important point advocating for efficient low-pressure catalysts for methanol synthesis. The choice of the feed temperature to the adiabatic reactor is critical in methanol synthesis because methanol synthesis is exothermic, and a temperature increase inside the reactor tends to promote the reverse water gas shift reaction. Figure S14 (d) illustrates the effect of varying the inlet temperature on the on parallel-series configuration (flowsheet 7) at various recycle ratios. The methanol production decreases as the feed temperature of the reactor is increased. A sharp decrease in methanol production is observed especially at lower recycle ratios (50%) compared to when the recycle is above 90%. The methanol production is higher at lower temperatures (e.g., T_{in} =200 °C). But due to low kinetics of CO_2 hydrogenation over the commercial catalyst at low temperature, a feed temperature slightly greater than 200 °C is adopted. It is also important to note the trend of the curve at recycle ratio of 90% (i.e., fraction = 10%). Under these conditions, most of the unconverted gases is recycled to the first two parallel reactors and consequently they have larger influence on the methanol production. Considering Figure 14 (d), the peak methanol production is observed at 210 °C, while variation of the inlet reactor temperature of R3 (which comes in series after the two parallel reactors) shows no significant effect on methanol production when long recycle is considered (see Figure 14 (f)). Thus, the feed temperature of adiabatic reactor in the range of 210°C <Tin <240 °C is preferred[12] when using the commercial catalyst and CO_2/H_2 feed. This is in line with the analysis presented by Cui et al. and Matthishke et al. in which the increase in recycle ratio decreases the hot spot temperature position within the reactor and consequently increase methanol production.[12-13] This is because higher space velocity for the gas into the single tube reactor results into lower single pass conversion and thus lower heat production. In the case of PtMeOH, with electricity sourced from variable wind and solar, it would be critical to check the temperature rise inside the reactor with changing space velocity, more especially at lower space velocity in which the reactants conversions tend to be high and thus resulting into higher heat production. On the other hand, lower superficial velocity results into poor heat transfer between the coolant and gas in the pipe. This could mean an added advantage of parallel reactor designs as they

can be made compacts and thus having a flexible range of allowable hourly space velocity. The effect of reactor length on the methanol production rate is shown in Figure S14 (e) and Figure S14 (g). The result indicates that increasing the length of the adiabatic reactors does not have significant impact on the methanol production rate, more especially beyond the reactor length of 2.5 m for the parallel-series configuration. This is because the methanol synthesis is dependent on the time to reach equilibrium and thus indirectly dependent on the reactor length. In simple terms, as shown in the figure S14 e, g and h, for parallel-series and series-series configuration, respectively, there is no added advantage of increasing the reactor lengths beyond 2.5 m for the parallel reactor and beyond 5 m for the series reactors. However, if the parallel reactors are designed to have a length below 2.5 m, the effect of reactor length is notable when the length of the third reactor (R3) is also decreased below 4.5 m. To dampen the effect of the reactor length while preventing the oversizing of the reactor, which is anticipated to influence the flexibility of the process, it is recommended to size the parallel-series reactors to be at least above 2.5 m for the scale studied in this paper. This is also supported by the reactor optimisation curves in section A5. Optimal reactor dimensions are also presented in Table S10 of section A5.1.

A4.2.2 Effect of fresh feed split and reactor length on the hot-spot temperatures and methanol production in a series and parallel-series reactor configurations.

The total feed mole flowrate into the reactor affects the local energy balance within the reactor. As previously discussed, the thermal management of the PtMeOH is a critical component of the process. The reaction of methanol synthesis is exothermic and thus temperature rise is expected, the highest temperature point of which is measured as hot-spot temperature at the reactor outlet in the case of an adiabatic reactor. The control of hot-spot temperature in methanol synthesis is very important and more especially under dynamic conditions as also deduced by Manenti et al.[14] Herein the effects of dividing the fresh feed to the reactors on the hot-spot temperatures in the series reactors with inter-stage cooling and separation, and parallel-series configurations are investigated. From Figure S15 (a), it is evident that the effect of splitting the fresh feed on the production rate for both configurations considered here is negligible. Temperature rise of the second reactor is steeper and higher than in the first reactor in the series configuration. When the total fresh feed is sent to the first reactor, the temperature of the first reactor drops significantly. Viewed in terms of residence time and conversion link, a high velocity to the first reactor (in case the total fresh feed is sent to the first stage resulting to a lower residence time), the conversion is low and therefore the heat evolution is reduced. While in the second and third reactor stages, the conversion is high and therefore more heat evolution and thus higher hot spot, vice-versa. However, for some fraction of the fresh feed to the first stage the hot spot temperature is high, indicating that for some ratio between the recycle and fresh feed, a different hot-spot position can be obtained in the first stage. The third stage in the series configuration seems not affected much by the fresh-feed flow split even in the case when part of the fresh feed is sent to this reactor. This analysis is based on a

fixed total fresh load level and recycle-purge ratio. An optimal recycle ratio with minimal hot spot positions in the reactor exists. In addition, scenario with dynamic load levels or wall-cooled reactors may present a different picture.

Considering Figure S15(b), the effect of feed split on the production rate for the parallel-series configuration shows that methanol production rate varies with having an additional fresh feed split. When the total fresh feed is sent to the third reactor (i.e., the case when there is no fresh feed sent to the first two parallel reactors), the methanol production rate is lower. On the other hand, when all the fresh feed is sent to the first two parallel reactors (i.e., the basic case where there is no fresh feed sent to the third reactor), the methanol production rate is at its highest value. Nonetheless, temperature is low at fresh-feed split equal to zero and high at fresh feed split equal 1, but both are still way below the maximum allowable hot spot temperature.

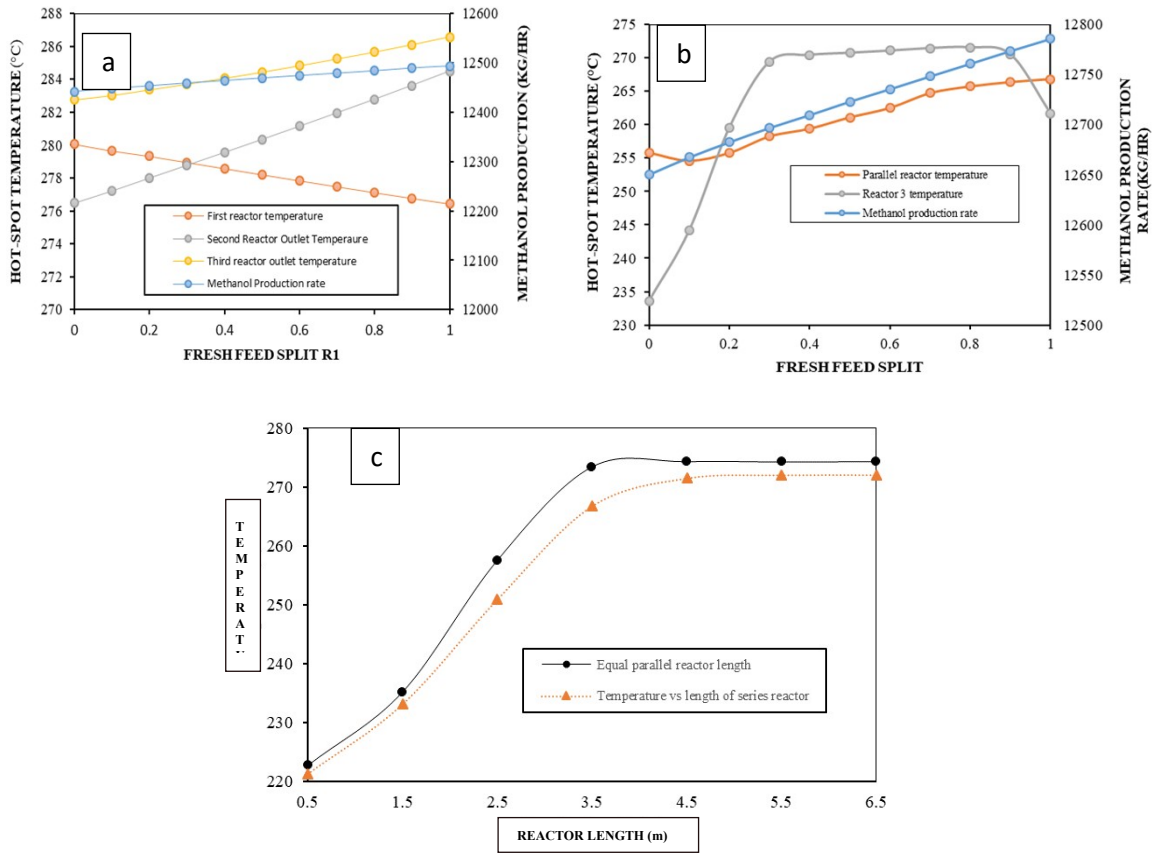

Figure S15: (a) Effect of feed split in a series configuration (Flowsheet 8). The CO_2/H_2 fresh feed is split between the first and second reactor. (b) Effect of feed split in a parallel-series configuration (flowsheet 7). The CO_2/H_2 fresh feed is split between the first two parallel reactors and third reactor which is in series with the parallel. The abscissa represents the feed ratio to the first reactor in a series configuration. (c) Effect of varying the length of the reactor on temperature change in the adiabatic bed. For this sensitivity the fraction =1-recycle was kept at Fraction =0.5.

In between the two extremes, an increasing trend in the temperature for the parallel reactors and series reactors is shown. Overall, this indicate that additional fresh feed split in the parallel configuration does not improve the production rate nor the temperature control. In the configurations presented in this work, all adiabatic reactors contain one single catalyst bed. Figure 15 (c) illustrates the variation of the temperature at the outlet of the adiabatic reactor with increase in the reactor length. The temperature change refers to the hot-spot in the adiabatic reactors. In this configuration, the hot spot temperature is below the upper hot spot temperature limit of T_{max} = 285 °C when T_{in} =210 °C (T_{out} ≈273 °C).[15] This indicates that the single-bed reactor, which is advantageously cheaper than water-cooled and gas cooled reactors, can be applied for CO_2 hydrogenation to methanol process in the process configurations and conditions of higher pressure (P = 75.7 bar) and commercial production scale as considered in this study.[12] The added advantage of the reactor is that it avoids detrimental possible internal condensation of methanol and water and increases the kinetics since the temperature inside the reactor is sufficiently high but below upper hot-spot limit. The temperature increase along the third reactor is lower than the first reactors due to the semi-equilibrium feed stream as most of the components are already converted in the first two adiabatic reactors. The findings in Figure S15(c) are in line with Rahmatmand et al. findings that the temperature rise in the adiabatic reactors precludes the gas condensate formation and consequently improves the catalyst durability.[16]

A4.3 Optimization of energy integration via Heat Exchanger Network (HEN) using pinch technology method

Overlooking heat integration tends to give underestimated results in terms of energy efficiency and process profitability.[17-18] Tsiklios et al. assessed the energy self-sufficiency of four prevalent power-to-X processes, i.e., power-to-hydrogen, power-to-ammonia, power-to-methane, and the power-to-methanol, without any consideration of process heat integration.[18] They deduced that 100% self-sufficiency (i.e., load coverage of 100% were not achieved in their respective scenarios and as a result, the energy had to be either imported in the form of electricity or as green energy carrier, or the energy supply capacity needs to be increased. In this section, a question of whether the integrated PtMeOH process excluding the CO_2 capture section, can achieve or be designed to achieve heat self-sufficiency is assessed via performing overall plant heat integration.[18]

One of the practical limitations of heat integration is the physical distance between the unit streams, practical limitations on heat transfer between different material phases (e.g., solid–liquid), and the trade-off between the heat exchanger cost and energy savings.[19] To optimize methanol synthesis, heat exchanger network design was considered to obtain minimum energy and operating costs. Using Aspen Energy Analyser, the minimum energy targets were set for flowsheet 7, 7B and 8. Figure S16 shows the composite curves for the corresponding flowsheets. The overall HEN of the SOEC-based PtMeOH was designed and optimised using pinch technology under steady state conditions. For this purpose, Aspen Energy Analyser is used, and the objective function adopted was to minimize the utility cost

which is formulated as a mixed integer linear programming (MILP) along with the corresponding minimum temperature difference (ΔT_{min}) of 10°C between cold and hot streams and taking into consideration the recommended design. Table S9 compares the three-flowsheet considering the utility requirements, number of shells, area, indicative operating, capital, and total costs for the original and optimal heat exchanger designs concerning each of these flowsheets. Flowsheet 7 has a relatively fewer number (up to 27) of heat exchangers.

	Flowsheet 7			**Flowsheet 7B**			**Flowsheet 8**		
Parameters	**Base case**	**Optimal HEN**	**Reduction %**	**Base case**	**Optimal HEN**	**Reduction %**	**Base case**	**Optimal HEN**	**Reduction %**
Heating utilities (kJ/h)	4.4×10^8	4.2×10^8	4.5	6.6×10^8	3.9×10^8	41.43	8.8×10^8	4.8×10^8	45.70
Cooling utilities (kJ/h)	1.6×10^8	1.4×10^8	12.5	3.9×10^8	1.1×10^8	70.7	5.5×10^8	1.5×10^8	72.90
Number of shells	57.00	62.00	-8.8	50.00	95.00	-90	63.00	164	-160
Total area(m^2)	1.5×10^4	1.6×10^4	-6.7	1.09×10^4	2.1×10^4	-91.8	1.9×10^4	4.6×10^4	-131
Operating cost ($/s)	0.889	0.875	1.6	1.058	0.824	22.1	1.21	0.884	26.7
Capital ($)	1.3×10^7	1.4×10^7	-7.7	1.25×10^7	1.5×10^7	-19.98	1.5×10^7	2.1×10^7	-46.3
Total Cost ($/s)	1.001	0.9897	1.13	1.19	0.978	17.55	1.35	1.10	18.7

Table S9: Parameters of the original HEN and optimal HEN.

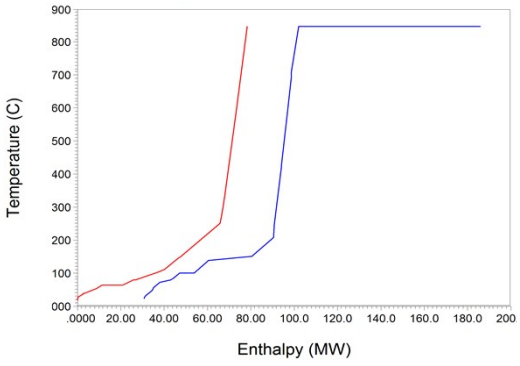

Figure S16(a): Flowsheet 7 composite curves

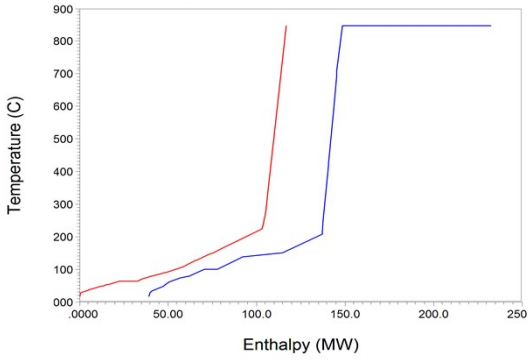

Figure S16(b): Flowsheet 7B composite curves

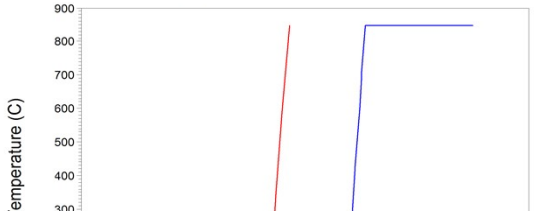

It is evident from Figure S16 and Table S9 that the SOEC-based PtMeOH process is dominated by heat demands, mainly for the SOEC feed streams. Flowsheet 7 has the smaller utilities requirements and hence total cost relative to flowsheet 7B and 8. It is critical to note that the cost calculation for the heat integration uses the default values from Aspen Plus Economics and this is done to get indicative values. The detailed cost analysis is beyond the scope of this work. The hot utilities are required for the region above the pinch, while the cold utilities are required in the region below the pinch point. For the SOEC-based PtMeOH configuration/flowsheet 7, heating utilities amounting to 365 MW is required and cooling utilities of 90.78 MW.

It is apparent that a slightly more heating and cooling utilities is required for flowsheet 7B. Thus, the parallel-series configuration needs less heating and cooling utilities in comparison to the series-based configurations for the base case. Nonetheless, the relative difference in terms of the total cost between flowsheet 7 and 7B is very small. But when the HEN was optimised, the series-based configuration represented by flowsheet 7B proved to be optimal in terms of utility requirements.

Thus, for the purpose of producing more methanol, flowsheet 7B or more simplified flowsheet 8 can be taken as the optimal looking at the combination of the previously discussed factors, even though flowsheet 8 uses slightly more utilities than the parallel-series-based flowsheet 7. All SOEC-based flowsheet shows dominance in heating utility requirements than the cooling utility requirement. The SOEC inlet stream cannot be heated to reach 850 °C by using the heat from the outlet stream of the SOEC and thus electrical heating was required to increase the temperature to 850 °C.

Thus, from this it is recommended to place the SOEC-based process near a reliable and cheap heat source e.g., typically available under a well-designed industrial cluster. All in all, the process requires a sophisticated HEN design, and it would be relevant to investigate its viability under flexible operation.

SECTION A5 OPTIMAL REACTOR AND DISTILLATION COLUMN DIMENSIONS

A5.1 Reactor dimensions and profiles

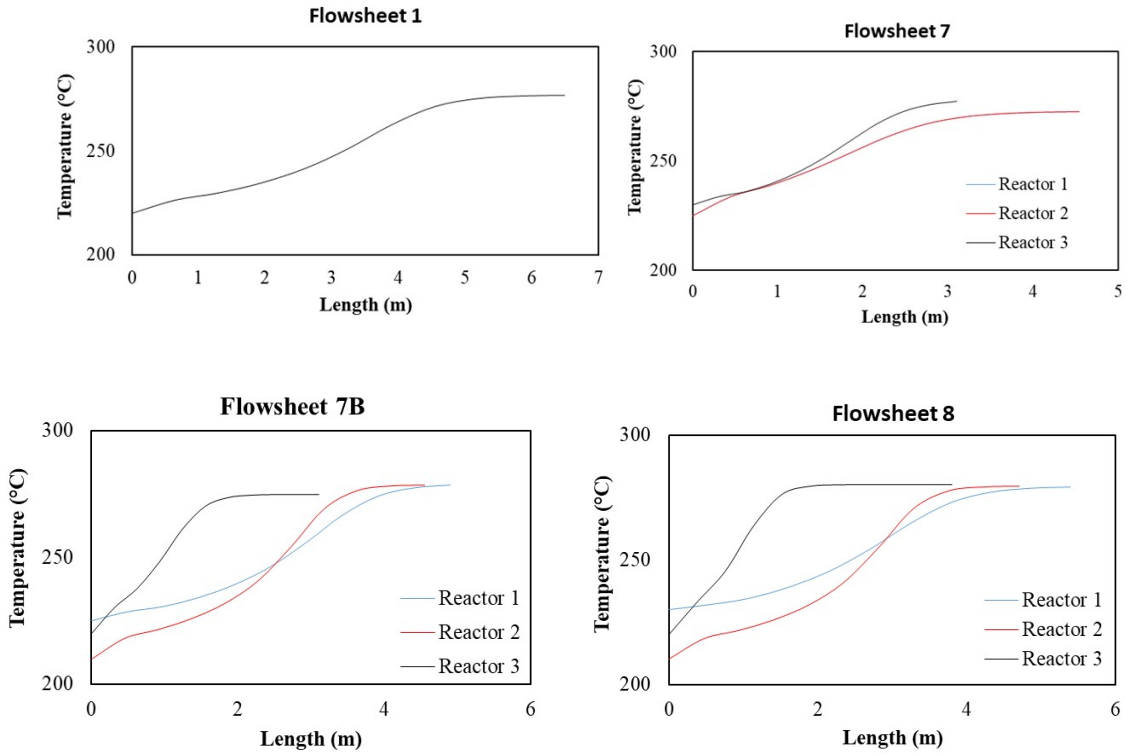

Figure S17: Temperature profiles for the reactors.

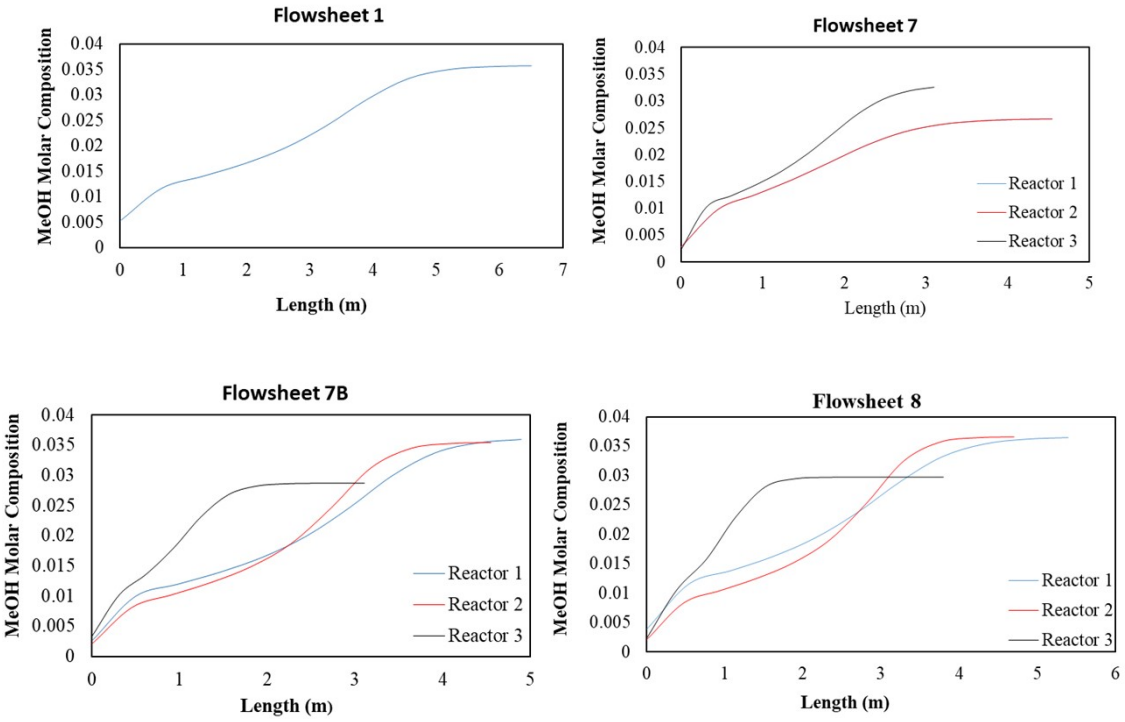

Figure S18: MeOH composition profiles for the reactors.

Table S10 Optimised adiabatic reactor dimensions

Flowsheet number	No. of Reactors	Length & Volume	Diameter
Flowsheet 1	1	Reactor 1 Length: 6.53 m Total volume: 54.2 m^3	Reactor 1: 3.25 m
Flowsheet 2	1	Reactor 1: 6.53 m Total volume: 54.2 m^3	Reactor 1: 3.25 m
Flowsheet 3	2	Reactor 1: 5.3 m Reactor 2: 5 m Total volume: 54.2 m^3	Reactor 1: 2.63 m Reactor 2: 2.55 m
Flowsheet 4	2	Reactor 1: 5.1 m Reactor 2: 4.9 m Total volume: 54.2 m^3	Reactor 1: 2.63 m Reactor 2: 2.63 m
Flowsheet 5	2	Reactor 1: 5.2 m Reactor 2: 4.8 m Total volume: 54.2 m^3	Reactor 1: 2.65 m Reactor 2: 2.6 m
Flowsheet 6A	2	Reactor 1: 5.1 m Reactor 2: 5.1 m Total volume: 54.2 m^3	Reactor 1: 2.6 m Reactor 2: 2.6 m
Flowsheet 6B	2	Reactor 1: 6.4 m Reactor 2: 2.23 m Total volume: 54.2 m^3	Reactor 1: 3.2 m Reactor 2: 1.25 m
Flowsheet 7	3	Reactor 1: 4.54 m Reactor 2: 4.54 m Reactor 3: 3.1 m Total volume: 54.2 m^3	Reactor 1: 2.5 m Reactor 2: 2.5 m Reactor 3: 2 m
Flowsheet 7B	3	Reactor 1: 4.85 m Reactor 2: 4.55 m Reactor 3: 3.11 m Total volume: 54.2 m^3	Reactor 1: 2.5 m Reactor 2: 2.4 m Reactor 3: 2 m
Flowsheet 8	3	Reactor 1: 4.66 m Reactor 2: 3.89 m Reactor 3: 3.5 m Total volume: 54.2 m^3	Reactor 1: 2.4 m Reactor 2: 2.4 m Reactor 3: 2.35 m
Syngas based flowsheet (co-electrolysis and eRWGS process)	3	Reactor 1: 5.4 m Reactor 2: 4.7 m Reactor 3: 3.8 m Total volume: 54.2 m^3	Reactor 1: 2.2 m Reactor 2: 2.2 m Reactor 3: 2.3 m

[1]The overall feed ratio before mixing with the recycle is kept at stoichiometric ratio of 3, so that the system never runs below the stoichiometric ratio.

A5.2 Distillation column sizing method

Tray type distillation column is selected following the literature history on methanol synthesis such as in the work of Van-Dal & Bouallou.[8] The distillation column (DC) using a partial condenser separates water as bottom product, a vapor distillate (lights), and methanol as high purity (>99wt%) top distillate. A warmer feed stream (80 °C) to the DC unit is used to reduce the reboiler duty. For green methanol

production, there are much less impurities in the crude methanol, and processes with 1–2 distillation columns are sufficient to produce fuel-grade methanol products.[10] The sizing assumes that the distillation column is isobaric—i.e., the pressure remains constant—and that the flow rates of liquid and vapor do not change throughout the column (i.e., constant molar overflow). The column was simulated with the rigorous model RadFrac in Equilibrium mode of Aspen Plus. In this paper detailed optimisation of the distillation column (e.g. encompassing tray spacing, etc.) is not performed, but the number of stages are taken to be similar to the work of Kiss et al.[11] for a CO_2 hydrogenation-based feed. This also is in close proximity with optimised stages (total stages in a range of 32 to 42 for a syngas feed) as performed by Luyben.[9] As also deduced by Luyben[9] rigorous determination of precisely the optimum number of stages following their optimisation, narrowing it down to a precision of a single stage, is unnecessary as it doesn't impact the cost that much and thus this was treated as beyond the scope of this work. The optimization of a column reflux and reboiler ratio was aimed towards higher production and an increase in quality of the product methanol. The sensitivity-based optimisation is simulated to get temperature, pressure, and composition profile and this is used to detect the operating parameters in Table 5 of the main article. The optimal feed stage was checked based by sensitivity analysis to determine the stage that reduces the boiler energy input.

NOMENCLATURE

d	m	Diameter of cylinder pellet
d_p^s	m	Diameter of sphere with equal specific surface area, for a cylinder $d_p^s = 3dh/(d+2h)$
h	m	Height of cylinder pellet
K	(-)	Equilibrium constant
N	(-)	The ratio of the tube diameter and volume-equivalent diameter, N=$2R_t/d_p^v$.
P	Pa	Pressure
r	mol/(kg_{cat}·s)	Reaction rate
R_t	m	Radius of reactor tube
Re_p^s	(-)	Reynolds number ($u\rho_f d_p^s/\mu_f$)
T	K	Temperature
u	m/s	Superficial gas velocity
Greek letters		
δ	m	Thickness of reactor wall
ε	(-)	Porosity of catalyst bed
μ_f	kg/m s	Gas viscosity
ρ_f	kg/m^3	Gas density
Subscripts		
0		Stagnant
f		Gas phase
p		Pellet
r		Radial

REFERENCE

1. K. Van den Bussche, G. Froment, A steady-state kinetic model for methanol synthesis and the water gas shift reaction on a commercial $Cu/ZnO/Al_2O_3$ catalyst. J. Cata. 161 (1996) 1–10.

2. G. H. Graaf, P. J. J. M. Sijtsema, E. J. Stamhuis and G. E. H. Joosten. Chemical equilibria in methanol synthesis. Chem. Eng. Sci. 41(1986) 2883–2890.

3. Leonie E. Lücking. Methanol Production from Syngas Process modelling and design utilising biomass gasification and integrating hydrogen supply, Master Thesis (2017), Delft University of Technology.

4. Zhu J, Araya SS, Cui X, Sahlin LS, Kær SK. Modeling and Design of a Multi-Tubular Packed-Bed Reactor for Methanol Steam Reforming over a Cu/ZnO/Al2O3 Catalyst. Energies 2020;13:610. https://doi.org/10.3390/en13030610.

5. Nguyen VH. Dynamic modelling of methanol synthesis from electrolytic hydrogen and captured carbon dioxide. Master's Thesis, LUT University. (2022)

6. Patcharavorachot Y, Chatrattanawet N, Arpornwichanop A, Saebea D. Comparative energy, economic, and environmental analyses of power-to-gas systems integrating SOECs in steam-electrolysis and co-electrolysis and methanation. Thermal Science and Engineering Progress. 2023 Jul 1;42:101873.

7. Chiou HH, Lee CJ, Wen BS, Lin JX, Chen CL, Yu BY. Evaluation of alternative processes of methanol production from CO2: Design, optimization, control, techno-economic, and environmental analysis. Fuel. 2023 Jul 1;343:127856.

8. Van-Dal, E.S. and C. Bouallou, *Design and simulation of a methanol production plant from CO2 hydrogenation.* Journal of Cleaner Production, 2013. **57**: p. 38-45.

9. Luyben, W.L., *Design and Control of a Methanol Reactor/Column Process.* Industrial & Engineering Chemistry Research, 2010. **49**(13): p. 6150-6163.

10. Cui X, Kær SK, Nielsen MP. Energy analysis and surrogate modeling for the green methanol production under dynamic operating conditions. Fuel. 2021 Sep.

11. Kiss AA, Pragt JJ, Vos HJ, Bargeman G, De Groot MT. Novel efficient process for methanol synthesis by CO2 hydrogenation. Chemical engineering journal. 2016 Jan 15;284:260-9.

12. Cui, X. and Kær, S.K., 2020. A comparative study on three reactor types for methanol synthesis from syngas and CO2. Chemical Engineering Journal, p.124632.

13. Matthischke S, Roensch S, Güttel R. Start-up time and load range for the methanation of carbon dioxide in a fixed-bed recycle reactor. Industrial & Engineering Chemistry Research. 2018 Apr 16;57(18):6391-400.

14. Manenti F, Cieri S, Restelli M, Bozzano G. Dynamic modeling of the methanol synthesis fixed-bed reactor. Computers & Chemical Engineering. 2013 Jan 10;48:325-34.

15. Voß JM, Duan T, Geitner C, Schluter S, Schulzke T. Operating behavior of a demonstration plant for methanol synthesis, Chemie Ingenieur Technik. 2022 Oct; 94(10): 1489-500.

16. Rahmatmand, B., Rahimpour, M.R. and Keshavarz, P., 2019. Introducing a novel process to enhance the syngas conversion to methanol over Cu/ZnO/Al2O3 catalyst. Fuel Processing Technology, 193, pp.159-179.

17. Ioannou I, D'Angelo SC, Galán-Martín Á, Pozo C, Pérez-Ramírez J, Guillén-Gosálbez G. Process modelling and life cycle assessment coupled with experimental work to shape the future sustainable production of chemicals and fuels. Reaction Chemistry & Engineering. 2021.

18. Tsiklios C, Schneider S, Hermesmann M, Müller TE. Efficiency and Optimal Load Capacity of E-Fuel-Based Energy Storage Systems. Advances in Applied Energy. 2023 Apr 23:100140.

19. Abbas A, Qadeer K, Al-Hinai A, Tarar MH, Qyyum MA, Ala'a H, Al Abri R, Lee M, Dickson R. Process development and policy implications for large scale deployment of solar-driven electrolysis-based renewable methanol production. Green Chemistry. 2022.